Monthly Notices of the ROYAL ASTRONOMICAL SOCIETY

MNRAS **508,** 2194–2203 (2021) https://doi.org/10.1093/mnras/stab2537
Advance Access publication 2021 September 13

Charge-exchange soft X-ray emission of highly charged ions with inclusion of multiple-electron capture

G. Y. Liang,[1]★ X. L. Zhu,[2] H. G. Wei,[1] D. W. Yuan,[1] J. Y. Zhong,[3] Y. Wu,[4,5] R. Hutton,[3] W. Cui,[6] X. W. Ma[2] and G. Zhao[1]

[1]*Key Laboratory of Optical Astronomy, National Astronomical Observatories, Chinese Academy of Sciences, Beijing 100101, China*
[2]*Institute of Modern Physics, Chinese Academy of Sciences, Lanzhou 730000, China*
[3]*Department of Astronomy, Beijing Normal University, Beijing 100875, China*
[4]*Key Laboratory of Computational Physics, Institute of Applied Physics and Computational Mathematics, P.O. Box 8009, Beijing 100088, China*
[5]*HEDPS, Center for Applied Physics and Technology, and College of Engineering, Peking University, Beijing 100871, China*
[6]*Department of Astronomy, Tsinghua University, Beijing 100084, China*

Accepted 2021 September 6. Received 2021 September 1; in original form 2021 June 18

ABSTRACT

Charge exchange has been recognized as a primary source of soft X-ray emission in many astrophysical outflow environments, including cometary and planetary exospheres impacted by the solar wind. Some models have been set up by using different data collections of charge-exchange cross-sections. However, multiple-electron transfer has not been included in these models. In this paper, we set up a charge-exchange model with the inclusion of double-electron capture (DEC), and make a detailed investigation of this process on X-ray emissions of highly charged carbon, nitrogen, oxygen, and neon ions by using available experimental cross-sections. We also study the effect of different *n*-selective cross-sections on soft X-ray emission by using available experimental *n*-distributions. This work reveals that DEC enhancement on line intensity is linearly proportional to the ratio of ion abundance in the solar wind. It is more obvious for soft X-rays from carbon ions (C^{4+}) in collision with CO_2, and the enhancement on line intensity can be up to 53 per cent with typical ion abundances [*Advanced Composition Explorer* (*ACE*)] in the solar wind. The synthetic spectra with parameters from the *Ulysses* mission for the solar wind reveal velocity dependence, target dependence, as well as the non-negligible contribution from the DEC.

Key words: atomic processes – line: formation – X-rays: general.

1 INTRODUCTION

Since the first discovery of X-ray and extreme ultraviolet emission from the comet C/Hyakutake 1996 B2 by Lisse et al. (1996) using the *Röntgen* satellite, there has been the thought whether this emission could be the result of charge-exchange (CX). Cravens (1997) first proposed that this kind of X-ray emissions could indeed be originated from CX processes between solar wind ions and cometary neutrals. Following this, such X-ray emission has been detected from most of the planets in the Solar system and proposed to be from solar wind ions by CX with planetary neutrals, e.g. Earth (Snowden, Collier & Kuntz 2004), Mars (Dennerl et al. 2006), Saturn (Branduardi-Raymont et al. 2010), Jupiter (Branduardi-Raymont et al. 2007), and Jovian (Hui et al. 2009). Lallement (2012) further proposed that the CX X-ray emission is a common feature at interfaces between a partially neutral gas and hot plasmas. This kind of charge-exchange emission (CXE) was observed at galactic supernova remnants, such as Puppis A (Katsuda et al. 2012) and Cygnus Loop (Katsuda et al. 2011), where hot ejecta/wind expands on to a cold ambient gas. Furthermore, CX X-ray emission was detected in some galaxies with star formation (e.g. M82 Liu, Mao & Wang 2011; Liu, Wang & Mao 2012), where hot outflows are driven by supernova explosions and stellar winds impact on ambient, and/or intergalactic medium. So the understanding of X-ray spectroscopy needs a sophisticated CX model besides collisional ionization equilibrium or non-equilibrium models (e.g. as in APEC, Smith et al. 2001; SPEX,[1] Kaastra, Mewe & Nieuwenhuijzen 2001) for many astrophysical observations, as mentioned above, to improve estimations of element abundance, ion/electron temperature, ionization age, and ionization stage in supernova remnants, as well as the structures of outflows in galaxies.

In order to fit X-ray spectral observations of objects, including comets, Bodewits et al. (2007) set up a CXE model with the inclusion of H- and He-like carbon, nitrogen, and oxygen ions by data compilation of cross-section. Based on a complete spectral data base, ATOMDB,[2] the CX model (namely ACX) of Smith, Foster & Brickhouse (2012) was used extensively for many kinds of astrophysical objects, as mentioned above, where the hydrogenic method was adopted to obtain the total CX cross-section, and the

★ E-mail: gyliang@bao.ac.cn

[1] www.sron.nl/astrophysics-spex
[2] www.atomdb.org

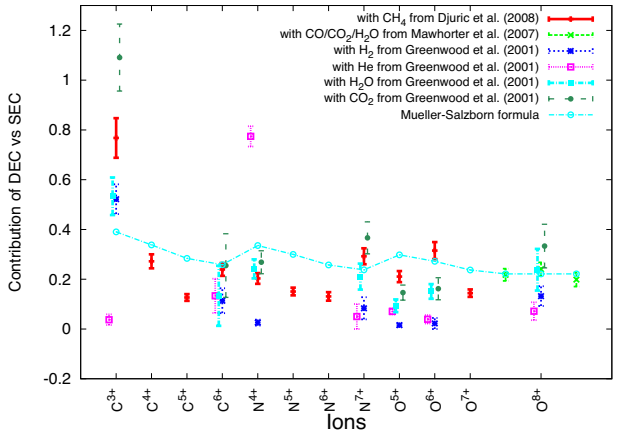

Figure 1. The fraction of DEC relative to SEC for different highly charged ions with data compilation from Greenwood et al. (2001), Mawhorter et al. (2007), and Djuric et al. (2008), and using the formula of Mueller & Salzborn (1977).

approximation of Janev & Winter (1985) was used to obtain the *nl*-resolved cross-section. Recently, the ACX model was updated by using the KRONOS data base,[3] which is a comprehensive CX data base. Liang et al. (2014) implemented a real-time calculation of CX cross-section by using parametrized multichannel Landau–Zener (MCLZ) theory to obtain CXE line emissivity. Cumbee et al. (2014, 2018) constructed a comprehensive CXE model (namely KRONOS[3]) by using realistic CX cross-section calculations, including the MCLZ, atomic–orbital close-coupling, molecular–orbital close-coupling, and classical trajectory Monte Carlo methods, where detailed comparisons have been performed with available measurements of charge-transfer cross-sections. In the KRONOS data base, the CX cross-sections with multi-electron targets (including H_2O, CO, CO_2, OH, and O) have been provided by using the MCLZ method (Mullen et al. 2016, 2017). By using various available CX cross-sections with the inclusion of experimental measurements, Gu, Kaastra & Raassen (2016) obtained several scaling laws for charge ($q-$), collision energy ($v-$), and main quantum number n-dependent cross-section, which significantly benefits a spectral modelling tool when the realistic calculation of CX is not available for some ions. However, all these reported CX models are based on single-electron captures (SECs). In the cometary and planetary atmospheres, molecular water, carbondioxide (CO_2), and methane (CH_4) are dominant donors in CX induced X-ray emissions. Many laboratory measurements have demonstrated that multiple-electron capture (MEC) plays an important role (Mawhorter et al. 2007; Djuric et al. 2008), as shown in Fig. 1. In the collision between O^{8+} and CO_2, the double-electron capture (DEC) cross-section occupies about ∼35 per cent. For lower charged C^{3+}, the double CX becomes particularly important in the solar wind/planetary atmosphere interaction.

In this work, we present a new CX model with the inclusion of a double CX process. In Section 2, we describe the physical model and the atomic data used in our model by data comparison. In Section 3, some results of CX spectra with the inclusion of DECs are presented. In Section 4, we give a summary and conclusion.

[3]www.physast.uga.edu/ugacxdb/

2 THEORY AND ATOMIC DATA

The CX model presented in this paper will be a part of the SASAL package, where the level energy and radiative decay rates are described in Liang et al. (2014). For SEC, available measurements have been compiled into the SASAL data base, as listed in Table 1. However, most CX cross-sections are total, and only a few measurements are n-selective cross-sections, including the recent new n-resolved CX cross-section obtained at the Lanzhou heavy-ion facility (Xu et al. 2021), where CX cross-sections over a wide collision energy range are measured. The experimental data are usually very limited considering the accessible collision energies and charge states; thus, theoretical evaluations over a wide energy range are indispensable for spectral modelling. Here, we used the scaling law formula (2) presented in Gu et al. (2016) and the fitting parameters therein as default in modelling.

In Fig. 2, we compare the CX cross-sections of highly charged oxygen ions ($O^{7+,8+}$) with hydrogen atoms from different theories, and available measurements with different neutrals. The SEC cross-section from fitting parameters of Gu et al. (2016) shows good agreement with the results of Shipsey, Green & Browne (1983, for O^{8+}) and the recommended data from Wu in private communication over a wide collision energy, where a quantum–mechanical molecular–orbital close-coupling (QMOCC) method was used (Wu et al. 2011). Below 200 km s^{-1} and/or above 3000 km s^{-1} of the collision velocity, the total cross-section from empirical formula (Wargelin, Beiersdorfer & Brown 2008), QMOCC (parametrized), and MCLZ calculations (as in KRONOS 3.1 data base), as well as the experimental values of Meyer et al. (1985) significantly deviates from the fitting of Gu et al. (2016) and Wu's recommended data. Above a collision velocity of 300 km s^{-1}, the QMOCC calculation shows a better agreement with those from the fitting of Gu et al. (2016) and the Wu's recommended data for O^{7+}. Below a collision velocity of 5000 km s^{-1}, the MCLZ calculation in KRONOS 3.1 shows a better agreement with other theories (e.g. the fitting of Gu et al. 2016, Wu's calculation, and the results of Shipsey et al. 1983) than that at a higher velocity for O^{8+}. So we select the scaling law and fitting parameters in Gu et al. (2016) as a default selection of SEC cross-section and its n-distribution of ion collisions with hydrogen and other neutrals in this work when experimental total SEC cross-sections and n-distribution are not available (here, the velocity-dependent cross-section and n-dependence on velocity are included). The n- or nl-selective CX cross-section from the KRONOS data base can be accessed and automatically matched to level energies and radiative decays in SASAL by a script of data import. When there is no experimental n-distribution or total cross-section for collisions with non-hydrogen targets, we also adopt the nl-selective cross-section from the KRONOS data base. In Fig. 2, available measurements with different molecules are plotted for comparison. There are obvious differences in collisions with different targets, which can be explained by the different ionization potentials of different molecules. However, these measurements are within the uncertainty of different calculations of oxygen ions with the hydrogen atom from different theories, except for the data with the He atom.

In order to explain the high-resolution spectra from present space missions and future missions [e.g. *Athena*[4] and the *Hot Universe Baryon Surveyor* (*HUBS*),[5] Cui et al. (2020)], The atomic data, including level energies and transitions decays, are stored in fine

[4]https://www.cosmos.esa.int/web/athena
[5]http://hubs.phys.tsinghua.edu.cn/en/index.html

Table 1. Collected CX data from available experiments.

Ions	Targets	Velocity/energy	Type	Reference
C^{q+} ($q = 3$, 5, and 6)	CO	$7q$ keV	Total[a]	Mawhorter et al. (2007)
C^{5+}	H_2O	$7q$ keV	Total[a]	Mawhorter et al. (2007)
C^{q+} ($3 \leq q \leq 6$)	CH_4	$7q$ keV	Total[a]	Djuric et al. (2008)
C^{q+} ($q = 3$ and 6)	H_2, He, H_2O, and CO_2	557/787[c]	Total[a]	Greenwood et al. (2001)
N^{q+} ($4 \leq q \leq 7$)	CH_4	$7q$ keV	Total[a]	Djuric et al. (2008)
N^{q+} ($q = 4$ and 7)	H_2, He, H_2O, and CO_2	599/792[c]	Total[a]	Greenwood et al. (2001)
N^{7+}	He, CO, CO_2, and H_2O	619/946[c]	n	Hasan et al. (2001)
N^{6+}	He		n	Zhu's exp[b]
O^{7+}	He, CO, CO_2, and H_2O	619/946[c]	n	Hasan et al. (2001)
O^{q+} ($5 \leq q \leq 8$)	CO	$1.5q/7q$ keV	Total[a]	Mawhorter et al. (2007)
O^{q+} ($5 \leq q \leq 7$)	CO_2	$1.5q/7q$ keV	Total[a]	Mawhorter et al. (2007)
O^{q+} ($5 \leq q \leq 7$)	CH_4	$7q$ keV	Total[a]	Djuric et al. (2008)
O^{q+} ($q = 5$, 7,and 8)	H_2, He, H_2O, and CO_2	648/722/772[c]	Total[a]	Greenwood et al. (2001)
O^{6+}	H_2O	$1.5q/7q$ keV	Total[a]	Mawhorter et al. (2007)
O^{6+}	H_2/He		n	Zhu's exp[b]
Ne^{q+} ($q = 7$ and 8)	H_2O, CO, and CO_2	$7q$ keV	Total[a]	Mawhorter et al. (2007)
Ne^{9+}	H, He, CO_2, and H_2O	$7q$ keV	Total[a]	Greenwood et al. (2001)
Ne^{8+}	H_2 & He	678/1072/1174/1238[c]	n	Zhu's exp[b]
Ne^{9+}	H_2 & He	657/929/1137/1737/2178[c]	n	Zhu's exp[b]

[a]Include multiple CX cross-section.
[b]Zhu's exp refers to the experimental measurements done in the Lanzhou Heavy Ion Research Facility.
[c]Collision velocity in units of km s^{-1}.

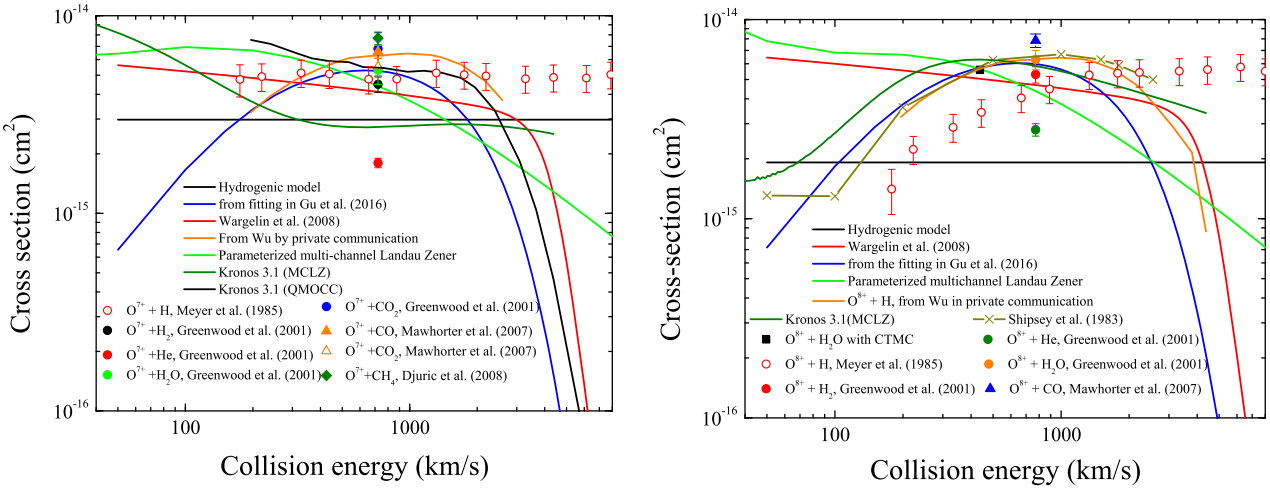

Figure 2. Comparison of CX cross-section of O^{7+} (left-hand panel) and O^{8+} (right-hand panel) impacting with the hydrogen atom from different theories (colour curves) and experimental values of Meyer et al. (1985), as well as with other neutrals from experiments (symbols with error bars).

structure in spectral models (e.g. APEC, Smith et al. 2001; SPEX, Kaastra et al. 2001), used extensively by the astrophysical community and SASAL (Liang et al. 2014). However, electron capture in heavy-ion collisions with neutrals is usually captured to a given quantum number n_q level, which can be written as

$$n_q = \sqrt{\frac{I_H}{I_t}} q \left(1 + \frac{q-1}{\sqrt{2q}}\right)^{-0.5}, \quad (1)$$

where I_H and I_t are the ionization potentials of H and other neutrals, respectively. And usually only total, n- or nl-resolved cross-sections are available. So level matching, grouping, and re-distribution procedures are necessary. In this work, such procedures could be performed, where the level index in the SASAL data base was first grouped into n-resolved. Then, these total, n- or nl-resolved cross-sections were automatically matched with corresponding level energies and radiative decay rates related to the quantum number of n_p/n, nl or nlS (here, S refers to total symmetry), and were redistributed to the captured ion with final fine-structure level states according to different distribution weights (including experimental n-distribution) by a script of data import. A similar procedure to that used in Smith et al. (2012) and Gu et al. (2016) is used for l-subshell distribution in this paper. For S- and final fine-structure-resolved cross-sections, statistical weight is adopted here.

For the cross-section of MEC, experimental data from the literature are used, as illustrated in Fig. 1. Formula (2) of Mueller & Salzborn (1977) gives a good rough estimation for MEC cross-sections, namely, $\sigma_{cx}^{k} = A_k q^{\alpha_k} I_t^{-\beta_k}$, where, $k = 2$ for DEC, q is the charge of highly charged ion, I_t is the ionization potential of neutrals in eV, and coefficients $A_k = 1.08 \times 10^{-12}$, $\alpha_k = 0.$, and $\beta_k = 2.80$. For other MEC cross-sections, the coefficient values can be found in table 1 of Mueller & Salzborn (1977). However, available realistic

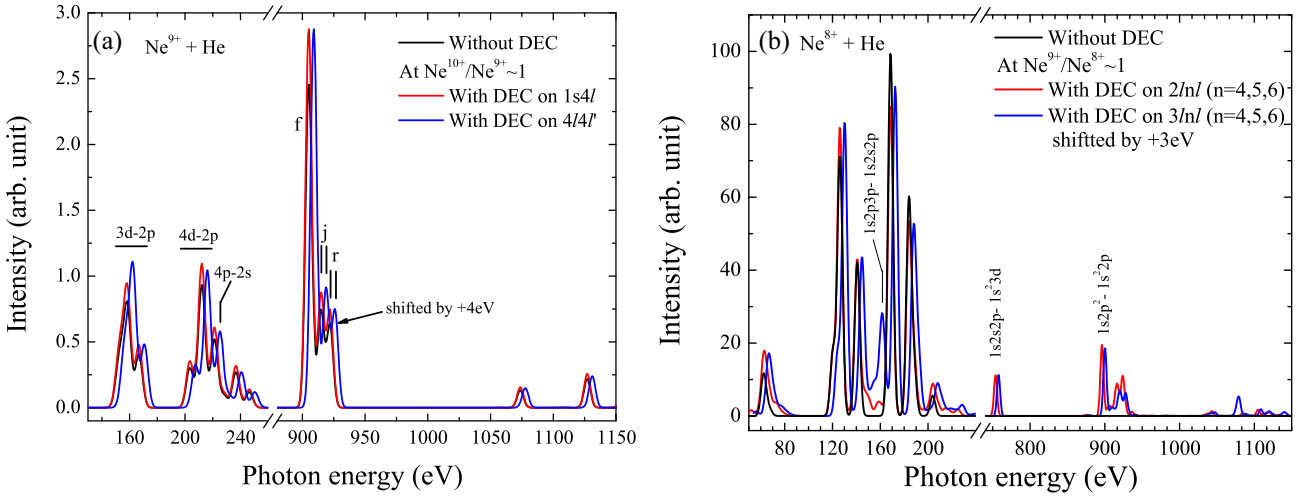

Figure 3. Panel (a): The CX spectrum of Ne^{9+} + He collision without and with DEC from Ne^{10+} on $4l4l'$ (blue, shifted by +4 eV for visualization) and $1s4l$ (red) channels at a collisional velocity of 1137 km s^{-1} and ion abundance ratio $\eta = \frac{Ne^{10+}}{Ne^{9+}} \sim 1$ used for DEC contribution. The DEC cross-section is from Flechard et al. (2001, fig. 9), while the *n*-selective SEC cross-section is from Xu et al. (2021). A linewidth of 5 eV is used in the Gaussian line profile. Panel (b): The CX spectrum of Ne^{8+} + He collision without and with DEC from Ne^{9+} on $3lnl'(n = 4–6)$ (blue, shifted by +3eV for visualization) and $2lnl'(n = 4–6)$ (red) channels at a velocity of 928 km s^{-1} and ion abundance ratio $\eta = \frac{Ne^{9+}}{Ne^{8+}} \sim 1$ used for DEC contribution. The DEC cross-section is 5.0×10^{-16} cm^2 from Greenwood et al. (2001), while the *n*-selective SEC cross-section is from Xu et al. (2021). A linewidth of 5 eV is used in the Gaussian line profile.

calculations for MEC are very scarce in published papers. So the formula of Mueller & Salzborn (1977) is used to estimate the total cross-section for ions without MEC data available. In the collision of Ne^{10+} with He, theoretical calculation and experiments reveal that the dominant channels of true DEC are $4l4l'$ (Flechard et al. 1997, 2001; Liu, Wang & Janev 2014; Ali et al. 2016). However, the data base used in most spectral models, including SASAL, does not include the $4l4l'$ excited states and subsequent decays from there. An independent particle model (IPM) is usually adopted in treating the DEC processes in highly charged ion collisions in which DEC can be considered as two separate SEC electrons, since the correlations effects between the two electrons are negligible except in the cases of resonant charge-transfer processes (Liu et al. 2014). Even in the case of quasi-resonant DEC processes of C^{4+}–He collisions, an IPM method works well and the electron correlation effects are found to be not important at the impact energies of a few keV u^{-1}, as shown in fig. 7 of Gao et al. (2017). By consideration of observed soft X-ray emissions result mainly from decays of single-excited states $n \leq 4$ to either the ground state or low-lying excited levels of He-like ions. An approximation of $1snl$ is considered to be the dominant channel in DEC, that is, one electron is captured to 1s, and the other is captured to nl orbital, where similar nl-selection as SEC (including its velocity dependence) is used as an approximation.

In order to validate the feasibility of this approximation, we calculate the doubly excited states ($2l3l'$, $2l4l'$, $3l3l'$, and $4l4l'$) of Ne^{8+} and cascade decays among them to lower levels (including singly excited states) by using AUTOSTRUCTURE (Badnell 1986).[6] The true DEC cross-section of Flechard et al. (2001) is allocated to $4l4l'$ or $1s4l$ channels by 'even'-distribution as SEC adopted by papers in Smith et al. (2012); Liang et al. (2014); Gu et al. (2016). We calculate the theoretical X-ray spectra of Ne IX (Ne^{8+}) following Ne^{9+} + He collisions as in the following discussion, and compare as shown in Fig. 3(a). There is no obvious difference for the resultant soft X-ray spectra [including He-like triplets, $1s2p\ ^1P_1 \rightarrow 1s^2\ ^1S_0$ (r), $1s2p\ ^3P_1 \rightarrow 1s^2\ ^1S_0$ (i), and $1s2s\ ^3S_1 \rightarrow 1s^2\ ^1S_0$ (f)] with the inclusion of DEC between $4l4l'$ and $1s4l$ cases. The cascade effect from doubly excited states of $4l4l'$ and singly excited states of $1s4l$ channels is comparable for the level population of $1s2/3/4l$ excited levels. So the approximation by allocating DEC cross-section on $1snl$ channels is feasible to predict DEC enhancement on CX line emissions of He-like ions. By using the *n*-allocation from equation (1) for collisions with non-hydrogen neutrals, we can predict the strong He-like triplets well, as discussed for n-manifold on X-ray in Section 3.1. In the collision of Ne^{10+} with He, $n_q = 4$ from equation (1) is consistent with the measurement by Flechard et al. (2001). So we believe this approximation for the DEC *n*-distribution is a feasible choice at present when realistic calculations are not available.

We further examine the above approximation in the collision of Ne^{9+} with He. Recent experimental measurements at a collisional velocity of 928 km s^{-1} (4.5 keV u^{-1}) revealed that the dominant channels of DEC are $3lnl'(n = 4–6)$ in the true DEC (Xu 2021). The SASAL data base includes $1s2lnl'$ doubly excited states for all Li-like ions with an atomic number $Z < 30$. In other words, in the DEC allocation, we can assume that one electron is captured to $2l$ and the other to nl'. Here, the true DEC cross-section (experimental value 5.0×10^{-16} cm^2 from Greenwood et al. 2001) is allocated to $3lnl'(n = 4–6)$ and $1s2lnl'$ channels by 'even'-distribution, respectively. The doubly excited states [$3lnl'$, $(n = 3–6)$] of Ne^{7+} and cascading decays to lower levels (including singly excited states) are calculated by using AUTOSTRUCTURE. Then we calculate the theoretical X-ray spectra of Ne VIII (Ne^{7+}) following Ne^{8+} + He collisions, and compare them, as shown in Fig. 3(b). There is no obvious difference for the $1s2p^2$–$1s^22p$ transition at 895 eV as well as emission lines from singly excited states below 200 eV. But an emission line at 158 eV and a weak line at 1075 eV from doubly excited states disappear in this approximate allocation on $1s2lnl'$. So the approximation by allocating DEC cross-section on $1s2lnl'$ levels included in the present data base, is acceptable to predict DEC's effect on CX soft X-ray emissions of Li-like ions with a nuclear number $Z < 11$. For abundant Li-like iron ions, this missing line due to DEC

[6] http://amdpp.phys.strath.ac.uk/autos/

will move to the soft X-ray region. A detailed calculation is necessary for the state-selective DEC cross-section. Additionally, there is an obvious difference between SEC and SEC-plus-DEC cases in that some emission lines appear with the inclusion of DEC. This can be used to identify the DEC in astrophysical observations.

In order to calculate the line emissivity of X^{q+}, due to SEC of $X^{(q+1)+}$ and DEC of $X^{(q+2)+}$ with neutrals or with lower charged ions, as well as subsequent radiative decays, either directly to the ground and lower excited states or via cascades, the density N_i of an ion with a charge of $q+$ at a given i th level state can be obtained by solving the following rate equation:

$$\frac{\mathrm{d}}{\mathrm{d}t}N_i^{q+} = \sum_{j>i} N_j^{q+}A_{ji} - \sum_{i<j} N_i^{q+}A_{ij} \tag{2}$$

$$+ n_{\mathrm{mol}} n_0^{(q+1)+}\left[C_{0i}(v) + \eta^{2\rightarrow 1}C_{0i}^2(v)\right], \tag{3}$$

where N_i^{q+} is the number density of $q+$ charged ions at the ith level state, while n_{mol} corresponds to the number density of neutral atoms/molecules. $C_{ij} \equiv <v\sigma_{\mathrm{cx}}(v)>$ and $C_{ij}^2 \equiv <v\sigma_{\mathrm{cx}}^2(v)>$ is single- and double-electron recombination rate coefficients, respectively. v is the relative collision velocity between $X^{(q+1)+}$ and neutrals, while $\sigma_{\mathrm{cx}}(v)$ and $\sigma_{\mathrm{cx}}^2(v)$ are the cross-sections of single-electron and double-electron transfer processes. $\eta^{2\rightarrow 1}$ refers to the ratio of ionic fraction between $q+2$ and $q+1$ charged ions before electron capture. Above complex coupled equations can be simplified to

$$\mathrm{d}\frac{\boldsymbol{N}}{\mathrm{d}t} = \mathbf{A}\boldsymbol{N}, \tag{4}$$

where $\mathbf{A}$ is a matrix being composed of parameters of various atomic processes mentioned above, and $\boldsymbol{N}$ is a one-dimensional vector of the number density N_i^{q+} of $q+$ charged ions. Here, an equilibrium assumption ($\mathrm{d}\frac{\boldsymbol{N}}{\mathrm{d}t} = 0$) is adopted to obtain the level population and further the line emissivity $\epsilon_{ij} = N_i A_{ij}$.

3 RESULTS

3.1 The effect of *n*-manifold on X-ray emission

Many theoretical calculations and laboratory measurements have demonstrated that the donors play an important role in the capture channels for n-selective cross-sections. There are differences not only in the total cross-section, but also in the apparent n-distribution of the captured electron among different collision neutrals. In Fig. 4, we compare the n-distribution of the captured electron in collisions of N^{7+} with different neutrals. According to the formula (1) and the fitting parameters presented in Gu et al. (2016), the peak capture channel is $n_{\mathrm{p}} = 4$. But laboratory measurements (Hasan et al. 2001) demonstrated a different n-distribution with a peak quantum number of five in the collision with CO, CO_2, and H_2O. For O^{8+} ions, the n-distribution of the captured electron shows a similar obvious difference, which is not presented here.

The resulting X-ray emissions are affected by the difference of n-distributions. The comparison of cross-sections presented in Fig. 2 demonstrates that the experimental cross-sections with different targets are within theoretical uncertainty of the ion collision with hydrogen atoms, but not the collision with He atoms . So we adopted the same total cross-section here, but the different n-distributions, including those obtained from formula (1) and available measured relative n-distributions, as well as that from the fitting parameters of Gu et al. (2016), show this effect by the X-ray spectra in $O^{7+,8+}$–H_2, and O^{7+}–He/CO/CO_2/H_2O collisions (see Fig. 5). For the Lyα line, the largest difference is about 17 per cent due to

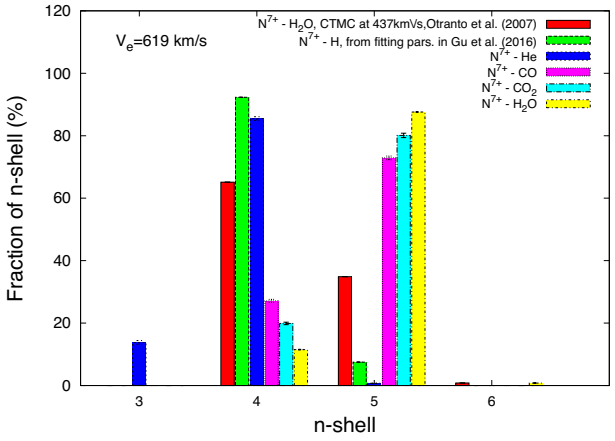

Figure 4. The n-distribution of the SEC at a velocity $V_{\mathrm{e}} = 619\,\mathrm{km\,s^{-1}}$ in the collisions of N^{7+} with different neutrals from Hasan et al. (2001, experiment), Otranto, Olson & Beiersdorfer (2007, theory), and Gu et al. (2016).

the difference of n-distributions. However, line emissivities of weak Lyγ and Lyσ are affected significantly by the n-distributions. We also notice strong soft X-ray emissions around ∼100–200 eV due to the cascade transitions of 3/4/5d → 2p of H- and He-like oxygen ion, and 3/4/5p → 2s of He-like ions. These emissions are important contributors to the ubiquitous diffuse soft (1/4 keV) X-ray background besides the hot gas within the local cavity (Smith et al. 2014). These line emissivities can change by factors, e.g. 4d → 2p line at 164 eV and 5d → 2p line at 183 eV in the collision of $O^{8+} + H_2$. The next-generation X-ray mission of *HUBS* (Cui et al. 2020) will cover the photon energy range of 100–2000 eV. Large uncertainty of these emission lines in the CX model will affect the spectral fitting to *HUBS* observation.

By using the available experimental n-distribution, we further compare the resulting X-ray emissions with that obtained by using the n-distributions as obtained from the collision of O^{7+} with He, CO, CO_2, and H_2O molecules, as shown in the right-hand panel of Fig. 5, where the same total cross-section from the fitting parameters of Gu et al. (2016) is used. There is no obvious difference between the strong helium-like triplets (Heα) and weak He$\beta\gamma$ lines. The largest difference of line emissivities is less than 2 per cent for the He-like triplets obtained by using different n-distributions. By using the n-distribution of He collision, the line emissivities of 3d/4d → 2p transition group lines change by 7–17 per cent. When using the n-distribution of multiple molecules, the line emissivities of 4d → 2p and 4p → 2s transition lines vary by up to a factor of 2, as well as 5d → 2p and 5p → 2s transition lines become strong X-ray contributors. This indicates that we can adopt the experimental n-distribution by using helium and/or H_2 to correct the theoretical n-selective cross-section of ions with the hydrogen atom in the CX model.

In Fig. 6, we show the comparison of He-like triplets of highly charged neon ions between different theories [with the n-distributions of a cross-section from two-centre atomic–orbital close coupling (TC-AOCC) and the fitting parameter of Gu et al. (2016)] and recent laboratory measurement of $Ne^{9+} + He$ collision at Lanzhou Heavy Ion Facility (Xu et al. 2021). There is almost no difference in strong X-ray emission from different n-distributions between the theory and experimental measurements. Several weak lines between 200 and 250 eV resulting from 4/5d → 2p and 4/5p → 2s transitions are predicted by using the TC-AOCC and experimental n-distributions. However, the n-distribution from the fitting parameters of Gu et al.

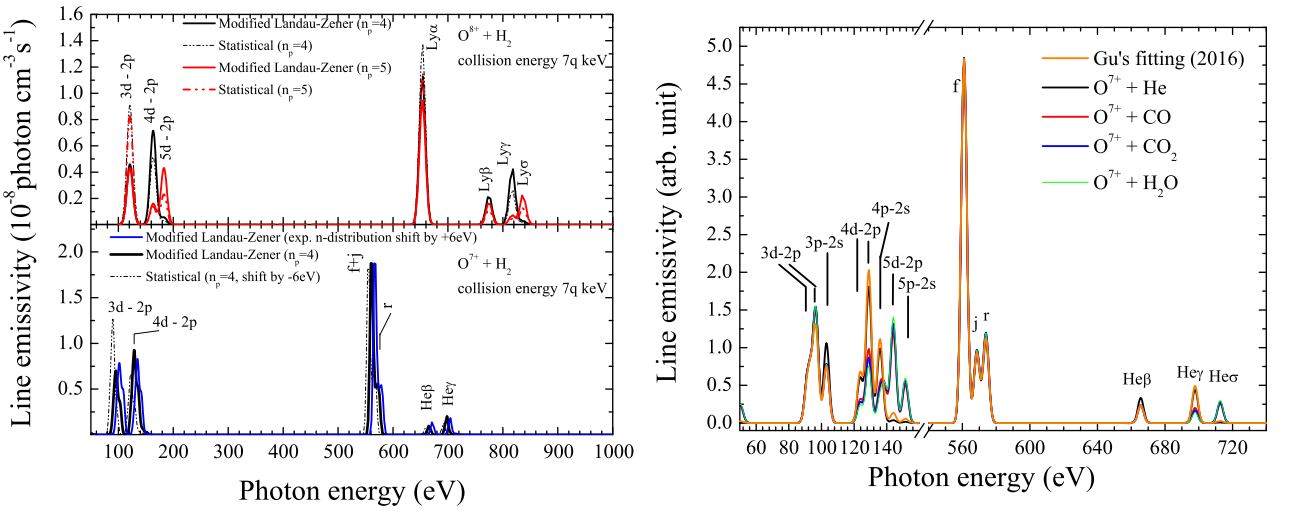

Figure 5. Left-hand panel: the CX spectrum of O^{8+} (upper) and O^{7+} (bottom) collision with H_2 by using the cross-sections from experiments of Greenwood et al. (2001), and by using different *n*-shell (from CTMC with peak fraction at $n_p = 5$ and from empirical value of $n_p = 4$) and *l*-shell distributions. The Gaussian line profile with a linewidth of 6 eV is used. Right-hand panel: the CX spectrum in O^{7+} collision with CO, CO_2, and H_2O molecules at a velocity of 619 km s^{-1} with the total cross-section from the fitting parameters of Gu et al. (2016) for the atom and different experimental *n*-distribution of Hasan et al. (2001) for other neutrals. MLZA is used for *l*-selection of the captured electron. A linewidth of 4 eV is adopted here.

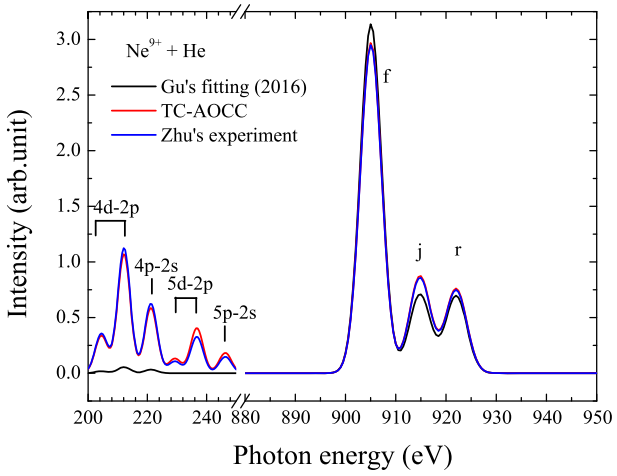

Figure 6. The CX spectrum of Ne^{10+} + He collision at a collisional velocity of 1137 km s^{-1}, where the total cross-section is from Greenwood et al. (2001), while the *n*-distribution is adopted from different methods, including the fitting parameters of Gu et al. (2016) for He, TC-AOCC calculation, and the experimental measurement at the Lanzhou heavy-ion facility (Xu et al. 2021). A linewidth of 5 eV is used in the Gaussian line profile.

(2016) for collision with He atom will result in very weak emissions from $n = 4, 5 \rightarrow 2$ transitions below 260 eV.

In summary, the reported model based on theoretical *n*-resolved cross-section or the peak capture channel of formula (1) is still credible for spectral modelling to present available X-ray observation with photon energy above 400 eV (e.g. *XMM–Newton* RGS observation). The emission lines arising from 3/4/5d → 2p to 3/4/5p → 2s transitions mentioned above are not observed with high resolution by the present space X-ray missions. The next-generation X-ray missions (e.g. *HUBS*[5] and *Athena*[4]) will cover a photon energy range of 100–2000 eV. The CXE model based on a simple electron capture channel of formula (1) is not appropriate for spectral modelling. The large difference by using different *n*-distributions reveals that the CXE spectra in this energy range are a good remote probe for the neutral components.

3.2 The effect of *l*-distribution on X-ray emission

In Fig. 5, we also compare the spectra with different *l*-distributions (e.g. the modified Landau–Zener and statistical models in this figure). Its influence can be up to 22 per cent for Lyα, and a factor of 2 for 3d → 2p at 121 eV, as well as 32 per cent for the $4d \rightarrow$ 2p at 164 eV with the same *n*-distribution. The large effect from *l*-distribution on high-resolution spectra reveals the urgent requirement of *nl*-resolved cross-sections for the CX model. This issue has been presented and discussed by comparison of laboratory X-ray spectra with theoretical spectra with different *l*-subshell distributions in the works of Mullen et al. (2017), Cumbee et al. (2018), and Xu et al. (2021). We will not extend this discussion in this paper. At different energy ranges, different approximations of *l*-distributions can give acceptable values as reported by Gu et al. (2016). Laboratory application of microcalorimeters with a high data collection area will give us more insight into the *l*-selection for the captured electron in the CX collision experiments of abundant carbon, nitrogen, and oxygen ions.

3.3 Contribution of DEC in X-ray emission

Fig. 1 shows that the cross-section of DECs occupies about ∼10–35 per cent versus that of SEC in collisions with molecules. Whittaker & Sembay (2016) presented the abundances of solar wind ions from the *Advanced Composition Explorer*(*ACE*) collected over a period of 13 years, including $O^{8+,7+}$ and $C^{6+,5+}$ ions. The scatter plots in that paper demonstrate that C^{6+}/C^{5+} can be up to unity, wherever O^{8+}/O^{7+} can be up to 35 per cent. In the explanation of cometary X-rays, Schwadron & Cravens (2000) adopted abundance values of O^{8+} and O^{7+} to be 0.07 and 0.2 for solar wind species in their CX model based on space *in situ* measurements taken by the *Ulysses* mission. For carbon ions ($C^{6+,5+}$), abundances of 0.318 and 0.210 were used, respectively.

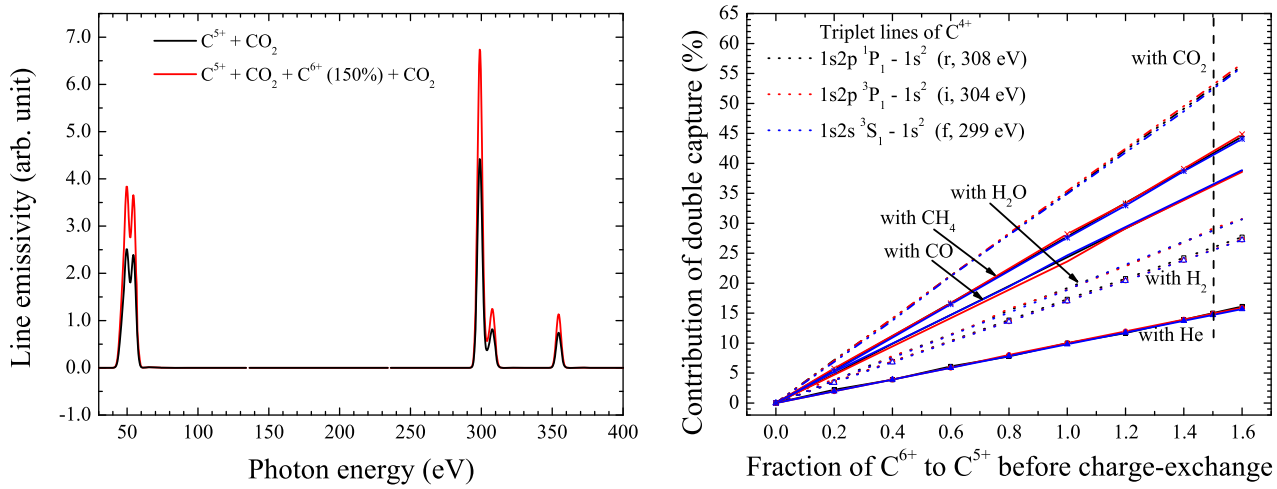

Figure 7. Left-hand panel: the effect of DEC on X-ray emissions of C V (C^{4+}) with 150 per cent bared C^{6+} relative to H-like C^{5+} ions in slow solar wind from Schwadron & Cravens (2000). A Linewidth of the Gaussian profile is 4 eV. Right-hand panel: enhancement contribution of DEC on He-like triplet lines versus the ionic fraction ratio (C^{6+}/C^{5+}) in the collision with He, H_2, CH_4, CO, CO_2, and H_2O at a velocity of 718 km s^{-1} with experimental SEC/DEC cross-sections. Vertical dashed line marks the ratio (1.5) of ionic fraction between C^{6+} and C^{5+} ions used in Schwadron & Cravens (2000).

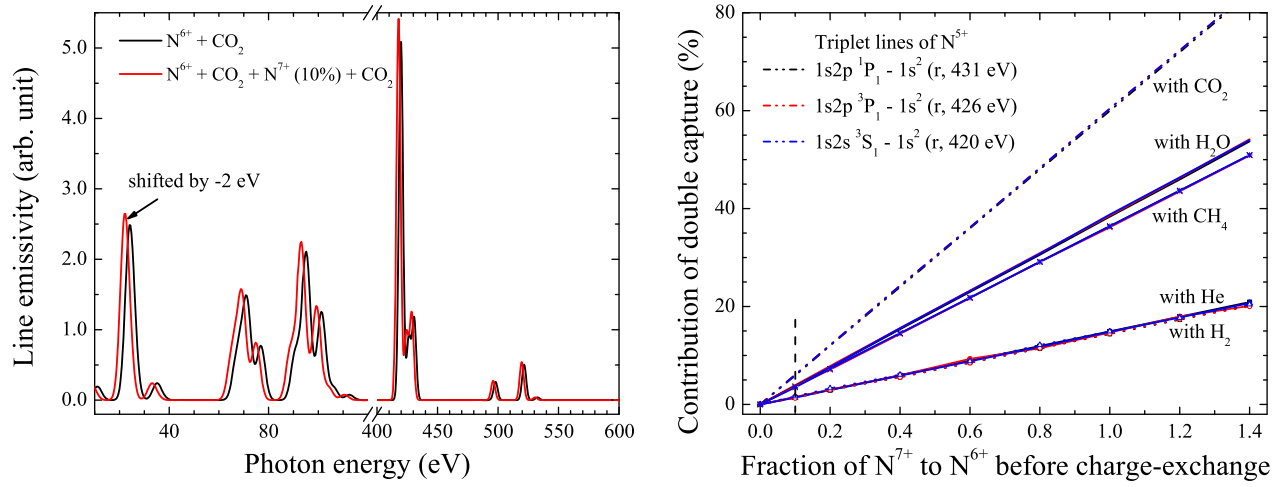

Figure 8. Left-hand panel: the effect of DEC on X-ray emissions of N VI (N^{5+}) with 10 per cent bared N^{7+} relative to H-like N^{6+} ions from the Schwadron & Cravens (2000). A Linewidth of the Gaussian profile is 4 eV. The spectrum with the inclusion of DEC is shifted by −2 eV for clarity. Right-hand panel: enhancement contribution of DEC on He-like triplet lines versus the ionic fraction ratio (N^{7+}/N^{6+}) in the collision with He, H_2, CH_4, CO, and H_2O at a velocity of 791 km s^{-1} with experimental SEC/DEC cross-sections. Vertical dashed line marks the ratio (10 per cent) of ionic fraction between N^{7+} and N^{6+} ions used in Schwadron & Cravens (2000).

Here, we investigate the contribution from DECs in CX X-ray emissions of highly charged carbon, nitrogen and oxygen ions by using available experimental cross-sections given in literature (Greenwood et al. 2001; Hasan et al. 2001; Mawhorter et al. 2007; Djuric et al. 2008), as shown in Figs 7–9. For different elements, different collision velocities are used here considering DEC cross-sections available at those values. Here, the experimental SEC cross-sections from the above literature are used. The enhancement from DEC on line intensity ($\delta\epsilon_{ij}$) is linearly proportional to the ratio of ion abundance ($\eta^{2\rightarrow 1}$) before electron captures. The linear fitting parameters are given in Table 2. In the collisions with complicated molecules (e.g. CO, CO_2, CH_4, and H_2O), the DECs have much more contribution in CX X-ray emissions of He-like triplets. The strongest one is the case of CO_2. By using the ion abundance reported by Whittaker & Sembay (2016) and that used by Schwadron & Cravens (2000) for highly charged carbon ions, the enhancement contribution from double-electron CX can be up to 53 per cent in the collision with CO_2. In comets, water (H_2O) is the dominant component. The DEC enhancement contribution from water is about 30 per cent. In the collision with an abundant element of He atom, the enhancement of triplet line intensities is about 15 per cent for C V (C^{4+}). For the strongest CX X-ray emissions, e.g. O VII triplets, the enhancement contribution from DEC is up to 10–12 per cent at the ratio of ionic fraction $\frac{X(O^{8+})}{X(O^{7+})} = 0.35$ [a typical value in solar wind, and used by Schwadron & Cravens (2000)] in the collision with CO_2. The DEC contribution is about 8 per cent in the collision with cometary donor – water. The solar wind abundance ratio is highly variable. A ratio of $\frac{X(O^{8+})}{X(O^{7+})} \sim 0.57 \pm 0.07$ was estimated by Snowden et al. (2004) from spectral line flux. The corresponding DEC enhancement will be up to ∼19 per cent. In the collisions with He and H_2, the contribution from DEC is negligible (less than 3 per cent). For N VI (N^{5+}) triplets, the enhancement contribution in solar wind with

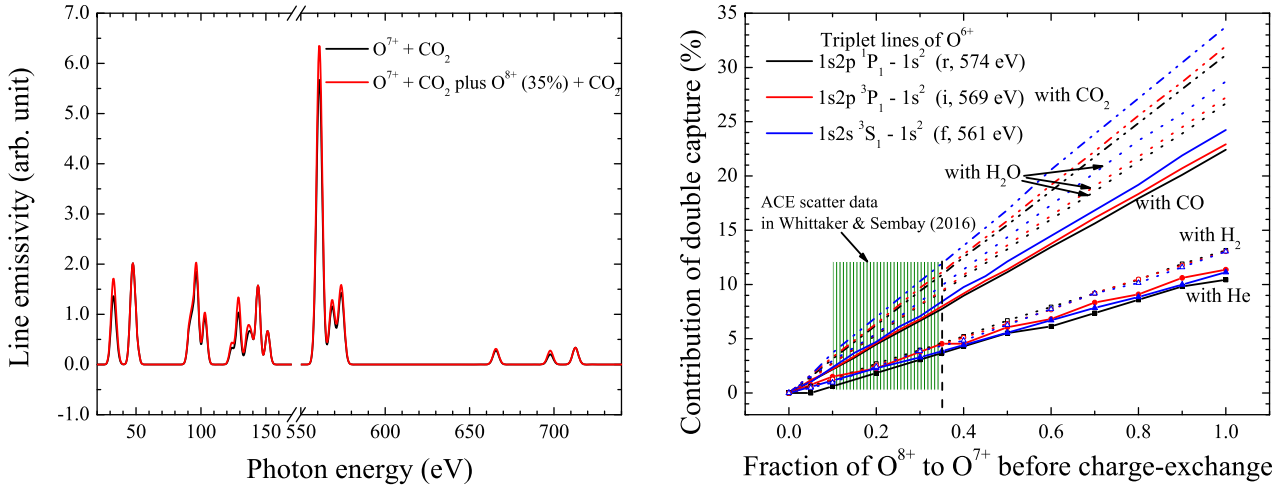

Figure 9. Right-hand panel: the effect of DEC on X-ray emissions of O VII with 35 per cent bared O^{8+} relative to H-like O^{7+} ions in solar wind from *ACE* data. A linewidth of the Gaussian profile is 4 eV. Right-hand panel: enhancement contribution of DEC on He-like triplet lines versus the ionic fraction ratio (O^{8+}/O^{7+}) in the collision with He, H_2, CO, CO_2, and H_2O at a velocity of 619 km s^{-1} with experimental SEC/DEC cross-sections. Vertical dashed line marks the ratio (0.35) of ionic fraction between O^{8+} and O^{7+} ions. Shadowed region indicates values of O^{8+}/O^{7+} to be ∼10–35 per cent from the scatter data plot in Whittaker & Sembay (2016).

Table 2. Values of fitting parameters ($\delta\epsilon_{ij} = a + b\eta^{2\rightarrow 1}$) of emission enhancement due to DEC.

Ions	Lines	Targets											
		H_2		He		CO		CO_2		H_2O		CH_4	
		a	*b*	*a*	*b*	*a*	*b*	*a*	*b*	*a*	*b*	*a*	*b*
C^{4+}	r	-2.10^{-10} ⋆	0.173 08	2.76^{-4}	0.0993	8.32^{-4}	0.2422	8.03^{-4}	0.3508	-1.14^{-5}	0.1920		
	j	7.02^{-4}	0.169 95	-1.61^{-4}	0.0997	−0.0021	0.2421	0.0	0.3540	7.75^{-5}	0.1914		
	f	2.10^{-10}	0.170 07	-2.67^{-10}	0.0980	0.0019	0.2425	-4.53^{-4}	0.3496	-1.25^{-3}	0.1921		
N^{5+}	r	-4.69^{-4}	0.144 28	6.47^{-10}	0.1493			-2.84^{-4}	0.5999	-5.35^{-4}	0.3837	-1.12^{-5}	0.3639
	j	-7.16^{-4}	0.144 47	1.28^{-3}	0.1455			5.94^{-4}	0.6027	9.14^{-4}	0.3856	-4.97^{-4}	0.3632
	f	2.22^{-3}	0.145 76	-4.83^{-4}	0.1482			5.94^{-4}	0.6027	-1.71^{-4}	0.3865	-4.43^{-4}	0.3644
O^{6+}	r	3.39^{-7}	0.131 65	-2.63^{-3}	0.1098	-5.43^{-4}	0.2245	-9.28^{-5}	0.3111	4.07^{-4}	0.2657		
	j	-8.70^{-4}	0.131 37	2.21^{-3}	0.1133	-3.38^{-4}	0.2299	4.24^{-4}	0.3185	-4.10^{-4}	0.2728		
	f	-1.92^{-3}	0.131 24	8.25^{-5}	0.1110	-4.81^{-4}	0.2423	1.34^{-3}	0.3374	-7.53^{-4}	0.2886		

⋆c^d denotes the value of $c \times 10^d$.

$\frac{X(N^{7+})}{X(N^{6+})} = 0.10$ (used by Schwadron & Cravens 2000) is less than ∼6 per cent.

Experimental DEC cross-sections are available only at one energy point for given collisions. The lack of theoretical calculations with the inclusion of MEC restricts the detailed studies on the velocity dependence of the CX X-ray emissions. The present investigation at a single energy point provides insight into the effect of X-ray emissions from DEC CX. For hot plasmas with much more bared ions relative to H-like ions, the contribution from DEC is more obvious, especially for carbon X-ray triplets.

3.4 Synthetic spectra of solar wind CX in comet

By using the ion abundance in the solar wind from the Solar Wind Ion Composition Spectrometer on *Ulysses* (Steiger et al. 2000; Schwadron & Cravens 2000), we calculate the CX emission spectra of solar wind ions impacting on H atom and water (H_2O) for slow and fast solar winds, as shown in Fig. 10(a). Fitting the RGS spectrum of the LINEAR comet determines the solar wind velocity to be $\sim 200 \pm^{85}_{45}$ km s^{-1} (Gu et al. 2016; Mullen et al. 2017). So we use the velocity of the solar wind to be 200 km s^{-1}. In order to show the velocity dependence of CX X-ray emission, the spectra of fast solar wind (700 km s^{-1}) are also plotted. The obvious difference reveals that the solar wind CX spectra are good probes to measure the velocity of the solar wind, as reported by Cumbee et al. (2018).

In the work of Mullen et al. (2017), the fitting to RGS spectra of the LINEAR comet with targets of H and H_2O combination can give a best fitting. Here we present the synthetic CX X-ray spectra resulting from the collisions with H atom and H_2O molecule for the slow solar wind (see Fig. 10b). The CX cross-section from KRONOS v3[3] is used for the H_2O target because experimental cross-sections are measured at velocities being close to fast solar wind. This figure demonstrates that some emission lines with the H_2O target are more enhanced than those with H atom. The Obvious ones are Lyα of C^{5+} and O^{7+} at 367 and 654 eV, He-like triplet of oxygen between 560 and 570 eV, as well as 3d/4d → 2p transition groups of carbon and oxygen ions at 50–150 eV, which will be covered by next-generation X-ray missions. Such a difference in CX emissions can help us to diagnose the composition of planetary atmosphere.

According to the ion abundance in slow solar wind from the work of Schwadron & Cravens (2000), we further calculate the synthetic spectra in the H_2O target with the inclusion of DEC (see the dark-green curve in Fig. 10b). There are obvious enhancements to the He-like triplet of carbon and minor enhancements to the He-like triplet

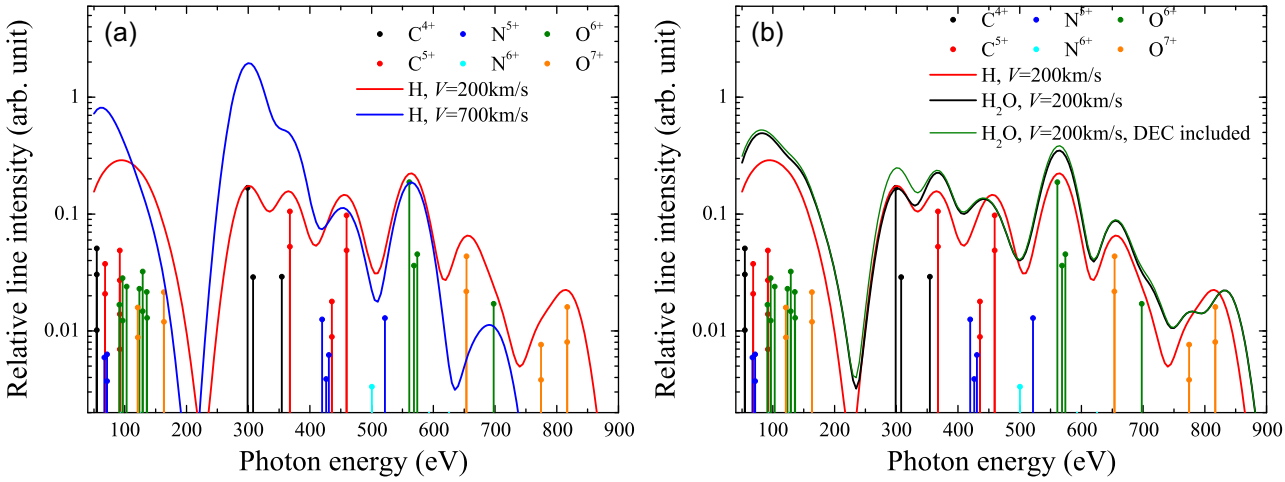

Figure 10. Theoretical X-ray spectra of H- and He-like carbon, nitrogen, and oxygen ions for the fast (700 km s^{-1}, blue curve) and slow (200 km s^{-1}, red curve) solar winds with an ionic fraction from Schwadron & Cravens (2000). Vertical colour lines with a top-symbol show the line emissivity of ions in slow solar wind. A linewidth of 50 eV is used with a Gaussian profile. Panel (a): The X-ray emissions are from collision with H atom. Panel (b): The X-ray emissions are from collision with H_2O (black curve) at a velocity of 200 km s^{-1}. The spectra from collision with H (red curve) are also overlapped for direct comparison. The dark green curve represents the CX spectra with the inclusion of DEC.

of oxygen. This again reveals that the contribution from MECs is not negligible in spectral fitting to real observation.

4 SUMMARY AND CONCLUSIONS

In summary, we set up a CX model with the inclusion of the DEC process. CX cross-sections from different sources (total, *n*-, *nl*- or *nlS*-selective) can be imported automatically into a data base by a script for comparisons. The effect of different n-selective cross-sections on X-ray emission was studied by using available n-distribution from measurements. For the strong Ly α line, the largest difference is up to 17 per cent from different predictions of peak main quantum number n_p. For He α lines, there is no obvious difference between theoretical and experimental n-distributions. Some line emissions arising from 3/4/5d $\rightarrow$ 2p and 3/4/5p $\rightarrow$ 2s transitions located around 80–200 eV are reported, and are significantly affected by n-distributions, especially those from compounds.

We further make detailed studies of DEC on X-ray emissions of highly charged carbon, nitrogen, oxygen, and neon ions by using available experimental cross-sections. The approximation of allocation of DEC cross-section on 1s*nl* is validated to be feasible for the calculation of soft X-ray emissions by the comparison of CX spectra of Ne^{9+} + He with the inclusion of DEC on the 1s4*l* (approximate) channel and 4*l*4*l*′ (physical) channel. For Li-like captured ions, the approximation of allocation of DEC cross-section on doubly excited states 1s2*nl*′ that is included in model data bases is also acceptable for the calculation of CX soft X-ray spectra. The unique feature from DEC in Li-like ions can be used to detect the DEC in observations. The DEC enhancement on line intensity is linearly proportional to the ratio of ion abundance in the solar wind. It is more obvious for X-rays of carbon ions (C^{4+}) in the collision with CO_2, and is up to 53 per cent with the typical ion abundance (*ACE* observation) of the solar wind. Synthetic spectra of solar wind ions impacting on cometary gas (including H atoms and H_2O molecules) are presented with the inclusion of DEC, which reveals the velocity-dependence and target-dependence of the CX X-ray emissions, as well as the non-negligible contributions from DEC in spectral fitting to real observations.

In conclusion, it is necessary to set up a complete CX model with benchmarked cross-sections, and with the inclusion of MEC to fit the requirement of the next-generation X-ray missions, e.g. *HUBS* and *Athena*. Detailed calculations of the MECs are an urgent requirement for a sophisticated CX model.

ACKNOWLEDGEMENTS

This work was supported by the National Key R&D Program of China, No. 2017YFA0402401, National Natural Science Foundation of China under grant numbers U1931140 and 11934004, Strategic Priority Research Program (B) of Chinese Academy of Sciences, No. XDB34020205, as well as Key Programs of the Chinese Academy of Sciences (QYZDJ-SSW-SLH050).

DATA AVAILABILITY

The data underlying this article are available in the article and in its online supplementary material.

REFERENCES

Ali R., Beiersdorfer P., Harris C. L., Neill P. A., 2016, Phys. Rev. A, 93, 012711
Badnell N. R., 1986, J. Phys. B: At. Mol. Opt. Phys., 19, 3827
Bodewits D., Christian D. J., Torney M., Dryer M., Lisse C. M., 2007, A&A, 469, 1183
Branduardi-Raymont G. et al., 2007, A&A, 463, 761
Branduardi-Raymont G., Bhardwaj A., Elsner R. F., Rodriguez P., 2010, A&A, 510, A73
Cravens T. E., 1997, Geophys. Res. Lett., 24, 105
Cui W. et al., 2020, in den Herder J. A., Nikzad S., Nakazawa K., eds, Proc. SPIE Conf. Ser. Vol. 11444, Space Telescopes and Instrumentation 2020: Ultraviolet to Gamma Ray. SPIE, Bellingham, p. 114442S
Cumbee R. S., Henley D. B., Stancil P. C., Shelton R. L., Nolte J. L., Wu Y., Schultz D. R., 2014, ApJ, 787, L31
Cumbee R. S., Mullen P. D., Lyons D., Shelton R. L., Fogle M., Schultz D. R., Stancil P. C., 2018, ApJ, 852, 7
Dennerl K. et al., 2006, A&A, 451, 709
Djurić N., Smith S. J., Simcic J., Chutjian A., 2008, ApJ, 679, 1661

Flechard X., Duponchel S., Adoui L., Cassimi A., Roncin P., Hennecart D., 1997, J. Phys. B: At. Mol. Opt. Phys., 30, 3697
Flechard X. et al., 2001, J. Phys. B: At. Mol. Opt. Phys., 34, 2759
Gao J. W., Wu Y., Sisourat N., Wang J. G., Dubois A., 2017, Phys. Rev. A, 96, 052703
Greenwood J. B., Williams I. D., Smith S. J., Chutjian A., 2001, Phys. Rev. A, 63, 062707
Gu L., Kaastra J., Raassen A. J. J., 2016, A&A, 588, A52
Hasan A. A., Eissa F., Ali R., Schultz D. R., Stancil P. C., 2001, ApJ, 560, L201
Hui Y., Schultz D. R. Kharchenko V. A., Stancil P. C., Cravens T. E., Lisse C. M., Dalgarno A., 2009, ApJ, 702, L158
Janev R. K., Winter H., 1985, Phys. Rep., 117, 265
Kaastra J. S., Mewe R., Nieuwenhuijzen H., 1996, in Silver. H. E., Kahn S. M., eds, 11th Colloquium on UV and X-ray Spectroscopy of Astrophysical and Laboratory Plasmas. Cambridge Univ. Press, Cambridge, p. 411
Katsuda S. et al., 2011, ApJ, 730, 24
Katsuda S. et al., 2012, ApJ, 756, 49
Lallement R., 2012, Astron. Nachr., 333, 347
Liang G. Y., Li F., Wang F. L., Wu Y., Zhong J. Y., Zhao G., 2014, ApJ, 783, 124
Lisse C. M. et al., 1996, Science, 274, 205
Liu J., Mao S., Wang Q. D., 2011, MNRAS, 415, L64
Liu J., Wang Q. D., Mao S., 2012, MNRAS, 420, 3389
Liu L., Wang J. G., Janev R. K., 2014, Phys. Rev. A, 89, 012710
Mawhorter R. J. et al., 2007, Phys. Rev. A, 75, 032704
Meyer F. W., Howald A. M., Havener C. C., Phaneuf R. A., 1985, Phys. Rev. A, 32, 3310
Mullen P. D., Cumbee R. S., Lyons D., Stancil P. C., 2016, ApJS, 224, 31
Mullen P. D., Cumbee R. S., Lyons D., Gu L., Kaastra J., Shelton R. L., Stancil P. C., 2017, ApJ, 844, 7
Müller A., Salzborn E., 1977, Phys. Lett., 62A, 391
Otranto S., Olson R. E., Beiersdorfer P., 2007, J. Phys. B: At. Mol. Opt. Phys., 40, 1755
Schwadron N. A., Cravens T. E., 2000, ApJ, 544, 558
Shipsey E. J., Green T. A., Browne J. C., 1983, Phys. Rev. A, 27, 821
Smith R. K., Brickhouse N. S., Liedahl D. A., Raymond J. C., 2001, ApJ, 556, L91
Smith R. K., Foster A. R., Brickhouse N. S., 2012, Astron. Nachr., 333, 301
Smith R. K., Foster A. R., Edgar R. J., Brickhouse N. S., 2014, ApJ, 787, 77
Snowden S. L., Collier M. R., Kuntz K. D., 2004, ApJ, 610, 1182
von Steiger R. et al., 2000, J. Geophys. Res., 105, 27217
Wargelin B. J., Beiersdorfer P., Brown G. V., 2008, Can. J. Phys., 86, 151
Whittaker I. C., Sembay S., 2016, Geophys. Res. Lett., 43, 7328
Wu Y. et al., 2011, Phys. Rev. A, 84, 022711
Xu J. W., 2021, PhD thesis, Univ. Chinese Academy of Science
Xu J. W. et al., 2021, ApJS, 253, 13

This paper has been typeset from a TEX/LATEX file prepared by the author.